Talanta 183 (2018) 114–121

Contents lists available at ScienceDirect

Talanta

journal homepage: www.elsevier.com/locate/talanta

A novel amperometric biosensor based on covalently attached multilayer assemblies of gold nanoparticles, diazo-resins and acetylcholinesterase for the detection of organophosphorus pesticides

Bin Jiang[a,*], Pei Dong[a], Jianbin Zheng[b]

[a] College of Urban and Environmental Science, Northwest University, 1 Xuefu Ave., Chang'an District, Xi'an 710127, Shaanxi Province, China
[b] Institue of Analytical Science, Northwest University, 1 Xuefu Ave., Chang'an District, Xi'an 710127, Shaanxi Province, China

ARTICLE INFO

Keywords:
Colloidal gold nanoparticles
Diazo-resins
Acetylcholinesterase
Layer-by-layer assembly
Covalently attached multilayer assemblies
Organophosphorus pesticides

ABSTRACT

Using an ionic layer-by-layer self-assembly technique, colloidal gold nanoparticles (AuNPs) and diazo-resins (DAR) were immobilised on the surface of a p-aminobenzenesulfonic acid-modified glassy carbon electrode to form a matrix composite membrane for acetylcholinesterase (AChE) immobilisation. Photo-sensitive DAR was used as the assembly interlayer to convert the ionic bond into a covalent bond to improve the biosensor stability. These fabrication processes were followed by electrochemical impedance spectroscopy and cyclic voltammetry to verify the membrane formation. Because of the introduction of AuNPs/DAR/AChE biofilms, the modified electrode exhibited excellent electron transfer mediation and electrical conductivity. In addition, it exhibited high sensitivity in the range of linear concentration from 1.0×10^{-8} to 1.0×10^{-12} g L^{-1} with the detection limit of 5.12×10^{-13} and 5.85×10^{-13} g L^{-1} for malathion and methyl parathion, respectively. More importantly, the presented biosensor considerably improved stability because the electrostatic interaction was converted into covalent bonds by UV irradiation. It is a simple, cheap and stable method for quantitative detection of organophosphorus pesticides, and this method may pave a way for the sensitive, simple detection of different analytes without the need of expensive instrumentation.

1. Introduction

Pesticides are widely applied to control the quantity of weeds, fungi, insects and other harmful pests to improve the yield of crops [1,2]. Organophosphorus pesticides (OPs) are used worldwide because of their high efficiency as insecticides, wide range of control and low cost. However, OPs can also cause environmental pollution to water, air, agricultural products and soil, and therefore negatively affect human health. Irreversible OPs inhibit the activity of acetylcholinesterase (AChE) and impact to the function of the central nervous system, eventually leading to respiratory paralysis and death [3,4]. Therefore, a method for the easy, sensitive, and rapid detection of OPs is very important for both human health and environmental safety [5]. There are many techniques that can be used to OPs detection, including spectroscopy [6], gas or liquid chromatography [7–10], mass spectrometry [11], fluorescence biological method [12], and enzyme-linked immune system analysis [13]. Many of these methods are selective and accurate, but are time-consuming and require expensive instrumentation. To solve these problems, biosensors with rapid response, low cost, and high specificity and sensitivity have been developed since the twentieth century.

Electrochemical biosensors based on AChE are particularly attractive detectors because of their fast reaction and high sensitivity [14,15]. At the electrode surface, fixed AChE can catalyse the hydrolysis of acetylthiocholine chloride (ATCl), producing the electroactive product thiocholine (TCh); this shows an irreversible oxidation peak at about 0.68 V [16,17], which signifies pesticide detection. However, the oxidation peak has high oxidation potential, which is weak, resulting in poor sensitivity. Hence, a major research focus seeks to develop an electrochemical biosensor based on AChE for improving the performance of biosensors, therein reducing oxidation potential [18].

Carbon-based nanomaterials, colloidal gold nanoparticles (AuNPs) [19], nanostructured conductive polymers, or composites have been extensively investigated to increase the porosity, specific surface area and conductivity of the electrodes and to create platforms for enhanced loading of AChE, enabling significant increase in biosensors sensitivity [20]. AuNPs are a focus for researchers owing to their performance: they are highly conductive, have good biocompatibility [21], and have served as a key element in the synthesis and catalysis of organic reactions in biomedicine [21,22] and sensing applications [23,24].

* Corresponding author.
E-mail address: jb1987@nwu.edu.cn (B. Jiang).

https://doi.org/10.1016/j.talanta.2018.02.016
Received 29 September 2017; Received in revised form 30 January 2018; Accepted 6 February 2018
Available online 15 February 2018

Furthermore, it has a lower oxidation potential and satisfactory selectivity compared to the other metals.

There have been many reports on various biosensors fabricated with AuNPs and AChE for the detection of OPs. A number of beneficial AChE immobilisation strategies have been developed based on the principles of encapsulation, physical adsorption and layer-by-layer self-assembly [25–29]. Among these methods, layer-by-layer self-assembly has been widely used because of its simplicity, low cost, wide selection of appropriate materials and precision of film composition control [30]. Layer-by-layer self-assembly by weak electrostatic force adsorption has been used to prepare enzyme biosensors in most previous studies; however, the stability of enzyme biosensors could be further improved through the strong covalent bond [31–33]. Thus, the purpose of this paper is to use layer-by-layer self-assembly technology to prepare stable covalently attached multilayer assemblies of P-ABSA/DAR/AuNPs/DAR/AChE (P-ABSA: *p*-acetamidobenzenesulphonyl azide) film in order to improve the stability of enzyme biosensors. Such a film would be an ideal material to detect OPs, having both a low detection limit and high sensitivity.

2. Experimental

2.1. Chemical reagents

Gold (III) chloride hydrate ($HAuCl_4$), Acetylcholinesterase (AChE 1000 U/mg) from electrophorus electrics (electric eel), Paraformaldehyde, Variamine Blue RT Salt and Acetylthiocholine chloride > 99% (ATCl) were purchased from Sigma Aldrich Phosphate buffered saline (PBS, pH 6.0) was prepared from KH_2PO_4, K_2HPO_4 and 0.1 M KCl. Sulfuric acid (H_2SO_4) and $ZnCl_2$ were purchased from Sinopharm Group Chemical Reagent Co., Ltd. P-amino benzene sulfonic acid was obtained from Aladdin reagent official website. In this study distillated water was used to obtain all solutions.

2.2. Apparatus

Electrochemical measurements were accomplished with a CHI660E (ShangHai Chenhua Co., China). The electrochemical cell consisted of a three-electrode system, the modified glassy carbon electrode (GCE) was used as the working electrode, Pt tablets acted as the counter electrode, and Hg/Hg_2Cl_2 electrode was applied as the reference electrode. All potentials in this paper were referenced to this saturated calomel electrode. The Portable UV-light WDH-204B (Shanghai Chi Tang Industrial Co., Ltd.) was applied to make the electrode Cross-linked. The decentralized and size of AuNPs was determined by transmission electron microscopy (TEM, Tecnai G2 S-twin of American company). UV–vis adsorption spectra were measured by Double-beam UV–vis spectrophotometer TU-1901 (Beijing Pu analysis of general instrument limited liability company).

2.3. Preparation of colloidal gold nanoparticles

Colloidal gold nanoparticles were prepared by citrate reduction of $HAuCl_4$ in aqueous solution in this paper [34]. All glass-ware was cleaned in a bath by freshly prepared 1:3 HNO_3: HCl, then rinsed thoroughly in distilled water and dried in air. Next, 0.425 mL 0.01% $HAuCl_4$ in the 25 mL round bottom flask was boiled under vigorous stirring. The color of the solution was changed from light yellow to burgundy when 1.70 mL of 1% sodium citrate was joined to the solution. Boiling was continued for 15 min; the heating mantle was then removed, and stirring was continued for an additional 15 min. The resulting solution of colloidal gold nanoparticles were stored in a brown bottle and kept at 4 °C after it reached room temperature.

2.4. Preparation of diazo-resins

Measured 6.6 mL sulfuric acid was put to a 50 mL conical flask, which was in an ice bath. The following steps were to avoid light. When the temperature dropped to 0–5 °C, the 50 mL conical flask containing sulfuric acid was added Variamine Blue RT Salt (3 g, 10 mM) under the condition of stirring. Appropriate amount of polyoxymethylene (0.36 g, 12 tendency) were added to 50 mL conical flask at 0–5 °C constant stirring 3 h. $ZnCl_2$ (2 g) were dissolved in 12 mL distilled water (releasing heat), placed in 4 °C for later use. After the completion of the reaction, $ZnCl_2$ solution was added to the reaction system, then the mixed system were placed in the refrigerator overnight at 4 °C. In the second day, the mixed solution was filtrated till the sediment layer cracked but did not turn black. The product was dissolved in 60 mL of non-water ethanol, and 60 mL of ether was added to extract the solid. The solid was finally washed twice with 100 mL of ether. After repeating the above steps, the solid product of yellow diazo-resins was dried at Vacuum overnight and stored in the refrigerator.

2.5. Preparation of covalently attached multilayer assemblies of P-ABSA/DAR/AuNPs/DAR/AChE

Glassy carbon electrode was first polished with 0.05 μm alumina slurry and rinsed thoroughly with distilled water. Then the electrode was successively sonicated in acetone and distilled water. The cleaned GCE was analysed in 5 mM P-ABSA solution containing 0.1 M KCl at a scan rate of 10 mV/s over a potential range of + 0.5–+ 1.4 V (SCE). The GCE was functionalised with P-ABSA by electrochemical modification to obtain a sulfonic-fuctionalised monolayer film [35]. After the modification, the modified electrode was sonicated in water for 10 min to remove the physically adsorbed materials. P-ABSA was found to have modified the surface of the GCE with negatively charged sulfonate groups. The electrode was placed in a 5 mL containing 0.3 mg/mL DAR solution soak for 15 min, the positively charged diazo groups of the DAR solution were adsorbed onto the electrode surface by electrostatic attraction interactions. Then the modified electrode was immersed in the AuNPs solution for 15 min. As DAR is positively charged, it would be adsorbed to negatively charged AuNPs by electrostatic layer self-assembly, thus preparing the GCE/P-ABSA/DAR/AuNPs modified electrode. After this, the modified electrode was immersed in the DAR solution for 15 min 5 μL containing 5 U of AChE solution coated with the modified electrode surface was stood for 30 min. AChE was dissolved in a pH 7.5 PBS solution; because the isoelectric point of AChE is 5.6 (pI = 5.6) with negative charge, it was easy to combine the positively charged DAR to form GCE/P-ABSA/DAR/AuNPs/DAR/AChE modified electrode by electrostatic interaction. Finally, the fabricated films were exposed to UV light for a given time to ensure completion of the reaction. The principle of covalent bond formation is as follows. It is well known that the diazonium group is very active and can decompose rapidly under UV irradiation or heating. The DAR used in this paper contains such diazonium groups. Cationic phenyl groups can be formed in polyion chains, which can react easily with nucleophilic compounds. Here, the sulfonate groups on the electrode surface, modified by P-ABSA, are nucleophilic. It can be inferred that sulfonate groups at the electrode surface react readily with the diazonium groups of DAR under UV irradiation. Moreover, the carboxylate groups on AuNPs surfaces are nucleophilic, and thus it is plausible that there is a photoreaction between the carboxylate groups on the AuNPs surfaces and the diazonium group of DAR. Similarly, the carboxylate groups on AChE can also react with the diazonium group of DAR under UV irradiation. In this way, the covalently attached multilayer films were obtained. The deposition process of the films was conducted in the dark to avoid the decomposition of DAR. Scheme 1 shows the processes of layer-by-layer self-assembly of covalently attached multilayer films on the GCE.

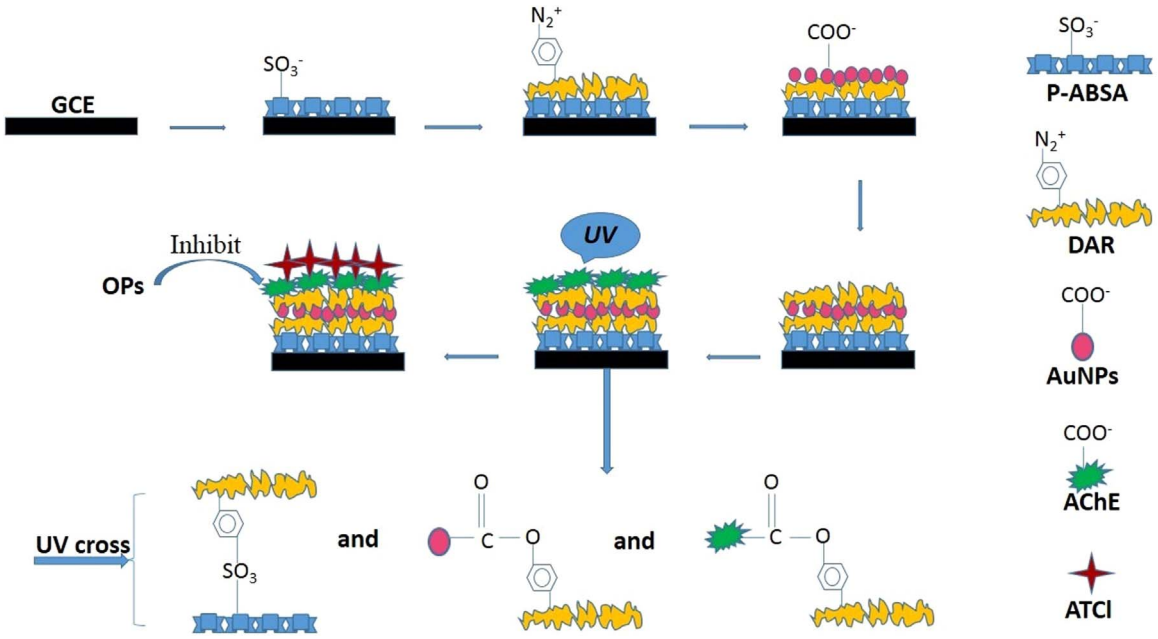

Scheme 1. Ideal assembling model of the covalently attached multilayer films containing DAR, AuNPs, and AChE on the GCE.

3. Results and discussion

3.1. Characterisation of AuNPs and DAR

AuNPs and DAR were characterised by UV–vis spectroscopy, and the absorption maxima were 522 and 377 nm (Fig. 1a–b), respectively. The UV peaks of AuNPs and DAR were approximately 520 and 380 nm, respectively. This result is similar to that obtained in previous articles [36,37], indicating that the synthesis of AuNPs and DAR was successful. Transmission electron microscopy observations indicated a particle diameter of AuNPs of 21 nm (Fig. 1c). The sizes of AuNPs are consistent with those reported in previous literature [34]. It could also be seen from Fig. 1(c) that the prepared AuNPs were uniformly dispersed and could be used for subsequent experiments.

3.2. Cyclic voltammetry in H_2SO_4 solutions

The deposition processes of DAR/AuNP bilayers were subsequently characterised by cyclic voltammetry (CV). Fig. 2 displays the CV curves of DAR/AuNP bilayers on a GCE in 1 M H_2SO_4 solutions. There was an oxidation peak at 0.48 V and a reduction peak at 0.35 V in the potential region from –0.1 to 1.4 V. However, in this potential range, no current response was observed on a bare GCE (Fig. 2a). The redox peaks are attributed to the existence of reversible redox transitions on the colloidal gold nanoparticles. From the Fig. 2(b–e), we could see that the higher the number of layers, the greater the peak current value. These data proved that the presence of AuNPs and the chemical reversibility on the surface reaction.

3.3. Cyclic voltammetry in $K_3Fe[CN]_6$ solutions

To check the electronic communication between immobilised AuNPs and the electrode, the electrochemical behavior of the electrode surface when modified with DAR/AuNPs bilayers was studied in $K_3Fe[CN]_6$ solution. $K_3Fe[CN]_6$ was subjected to a reversible electrochemical reaction on various electrodes and was widely used as an electrochemical probe to detect the properties of the film on the surface of the peak. From Fig. 3(a), we could see that $K_3Fe[CN]_6$ exhibited almost reversible behavior on bare GCE. After the electrodes were made with P-ABSA, an insulating layer having many anions on the GCE was produced. It introduced barriers to electron transfer at the interface. This was reflected by the disappearance of the current response for $K_3Fe[CN]_6$, there was nearly no obvious current response for $K_3Fe[CN]_6$ in Fig. 3(f). However, after modification with one bilayers of DAR/AuNPs, the redox peaks of $K_3Fe[CN]_6$ were again observed in Fig. 3(b), indicating that the AuNPs improved the electron transfer between $K_3Fe[CN]_6$ and the electrode. Compared with a bare GCE, however, the obtained current response was smaller. This might be due to the presence of poorly conductive DAR. Furthermore, there was a repulsion interaction between the AuNPs with negative charge and K3Fe[CN]6. From Fig. 3(b–e), it is clear that all current responses were smaller compared with the instance of one layer of DAR/AuNP, and this may be the result of nonconductive DAR and the effect of film thickness.

3.4. Electrochemical impedance spectroscopy of various modified electrodes

The electronic communication between GCEs and immobilised AuNPs was further studied by electrochemical impedance experiments in order to obtain further kinetic information. Fig. 4 shows the electrochemical impedance spectroscopy of GCEs modified with P-ABSA and DAR/AuNPs with different bilayer numbers (n), and also the bare GCE. It could be seen that the exposed objects were almost straight, and almost no distinct semicircle shape could be observed in Fig. 4(a), which indicated very small electron transfer resistance existence. The appearance of a large semicircle (Fig. 4e) after the GCE was modified by a layer of P-ABSA indicated that the electron transfer resistance here was greatly increased because of the nonconductive nature of P-ABSA. When the GCE was modified with a layer of DAR/AuNPs, the semicircle diameter decreased dramatically due to the existence of AuNPs in Fig. 4(b) and increased again with the increasing layer numbers of DAR/AuNPs because of the nonconductive DAR and the effect of film thickness in Fig. 4(c and d). These data were consistent with CV experiments results. Furthermore, with raised numbers of DAR/AuNPs, the increase of the semicircular diameter does not change, which means that the assembling process is uniform and continuous.

3.5. Selection of experimental conditions

3.5.1. The effect of pH

The CV results of GCE/P-ABSA/DAR/AuNPs/DAR/AChE in 0.1 M

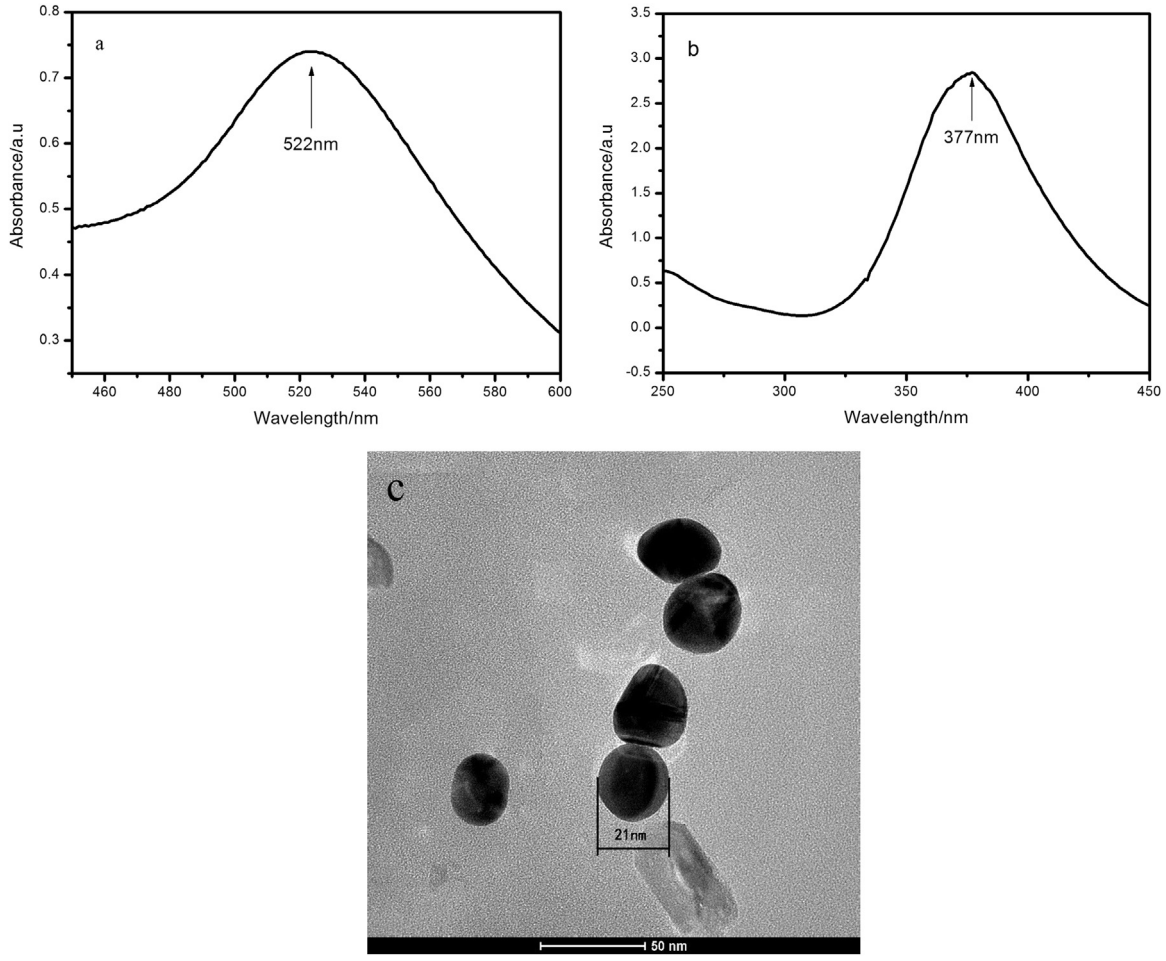

Fig. 1. a, 1b: UV–vis absorption spectra of AuNPs and DAR. **c:** TEM image of AuNPs.

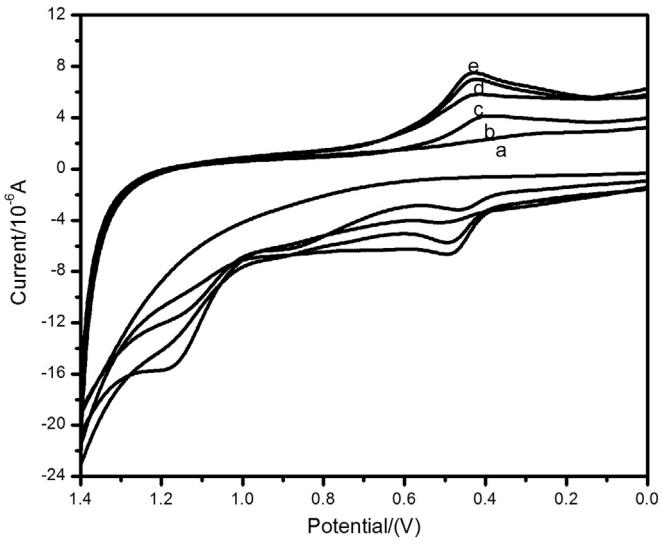

Fig. 2. CVs of: bare GCE (a); GCE/P-ABSA/DAR/AuNPs (b); GCE/P-AB SA/(DAR/AuNPs)$_2$ (c); GCE/P-ABSA/(DAR/AuNPs)$_3$ (d); GCE/P-ABSA/ (DAR/AuNPs)$_4$ (e) in 1 mM solution. Scan rate: 100 mV/s.

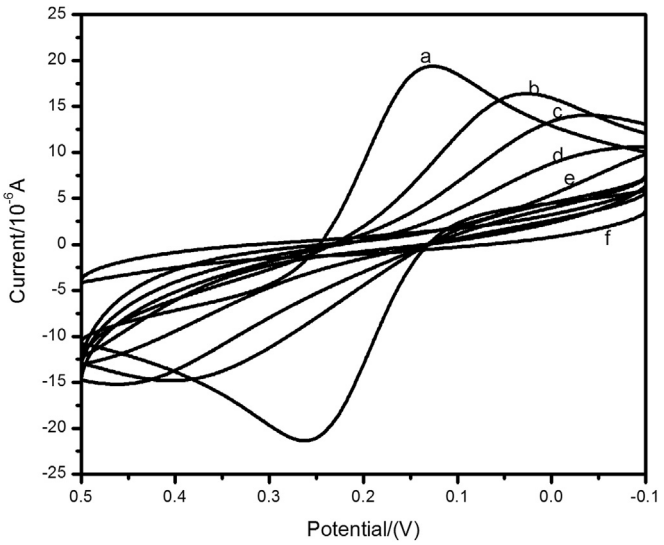

Fig. 3. CVs of 1 mM $K_3Fe[CN]_6$ and 1 mM $K_4Fe[CN]_6$ containing 0.1 M KCl at: bare GCE (a); GCE/P-ABSA/DAR/AuNPs (b); GCE/P-ABSA/(DAR/Au- NPs)$_2$ (c); GCE/P-ABSA/(DAR/AuNPs)$_3$ (d); GCE/P-ABSA/(DAR/AuNPs)$_4$ (e). GCE/P-ABSA (f); Scan rate: 100 mV/s.

PBS containing 1 mM ATCl with pH values varying between 5.0 and 7.0 are presented in Fig. 5. It was found that the oxidation peak current increased with increasing pH of PBS, reaching its maximum at 6.0, and then decreased with the subsequent increase of pH. This might be due to the presence of AChE, which isoelectric point was 5.6. It would be deactivated with improper pH. Herein, the pH 6.0 PBS was chosen as the supporting electrolyte for the detection with the consideration that this pH relatively approached the environmental pH.

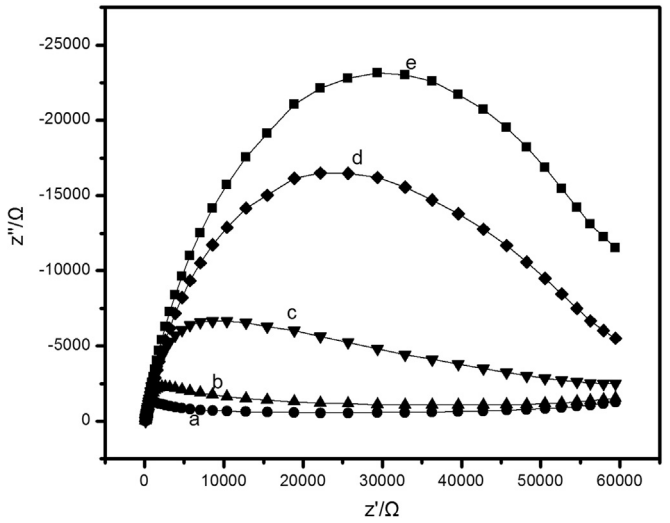

Fig. 4. Complex impedance plots in 5 mM $Fe(CN)_6^{3-/4-}$ containing 0.1 M KCl at: bare GCE (a); GCE/P-ABSA/DAR/AuNPs (b); GCE/P-ABSA/$(DAR/Au\text{-}NPs)_2$ (c); GCE/P-ABSA/$(DAR/AuNPs)_3$ (d); GCE/P-ABSA (e); The frequency range is 10^{-1}–10^{-5} Hz.

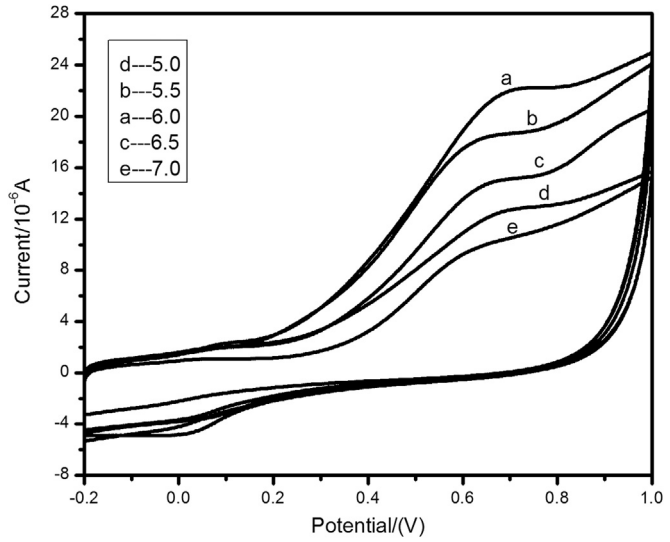

Fig. 5. CVs of GCE/P-ABSA/DAR/AuNPs/DAR/AChE in 0.1 M PBS containing 1 mM ATCl with the pH values varying from 5.0 to 7.0.

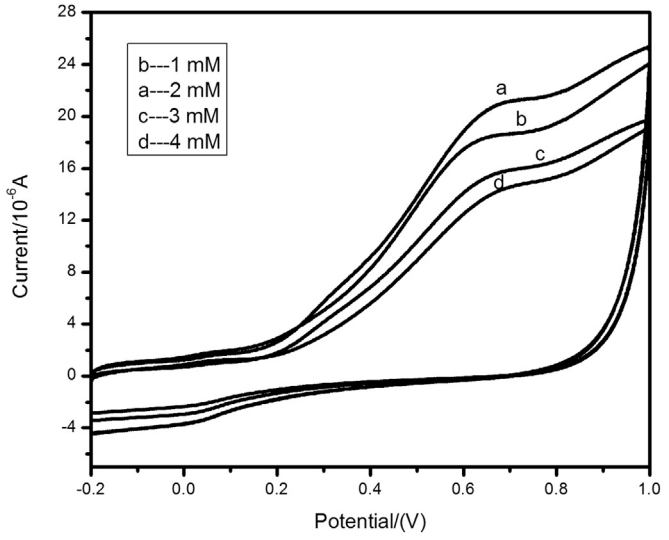

Fig. 6. CVs of GCE/P-ABSA/DAR/AuNPs/DAR/AChE in 0.1 M PBS (pH 6.0), ATCl concentrations are respectively 1 mM/2 mM/3 mM/4 mM.

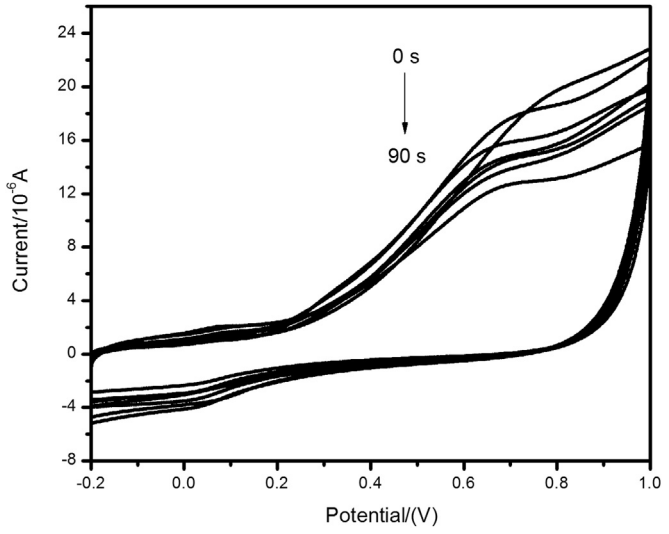

Fig. 7. CVs of GCE/P-ABSA/DAR/AuNPs/DAR/AChE in 0.1 M PBS (pH 6.0) containing 2 mM ATCl, the UV crosslinking time is 0 s/15 s/30 s/45 s/60 s/75 s/90 s.

3.5.2. The effect of Substrate concentration

In this paper, the response current signal about different concentrations of ATCl in 0.1 M PBS (pH 6.0) buffer solution was investigated, and the experimental results were shown in Fig. 6. The catalytic current increased together with increasing concentration of ATCl, which was varied between 1 and 2 mM. When the ATCl concentration was 2 mM, the current response reached its maximum; however, when the ATCl concentration was more than 2 mM, the current response decreased. This was because the increased ATCl concentration caused the enzyme activity centre to be gradually occupied by the substrate. Therefore, 2 mM ATCl solution was selected as the ideal substrate concentration for the determination of OPs.

3.5.3. The effect of UV crosslinking time

The relationship between UV crosslinking time and current response was also investigated over the range of 15–90 s. The results of these experiments are shown in Fig. 7, indicating that the UV crosslinking time increased with the reduction of current. However, when the UV crosslinking time was greater than 15 s, the peak was slightly reduced, because the resistance of the covalent bond of AuNPs and DAR on the GCE surface could decrease the transfer of electrons. At a UV crosslinking time of 15 s, ionic bonds could not be completely converted to covalent bonds, resulting in the instability of the composite film. However, for a UV crosslinking time of greater than 60 s, the activity of the enzyme was reduced because of prolonged exposure to UV light, and therefore the sensitivity of the biosensor was decreased. Consequently, a UV crosslinking time of 30 s was selected for this research.

3.6. The effect of potential scan rate

GCE/P-ABSA/DAR/AuNPs/DAR/AChE electrode with different scan rates (20–160 mV/s) was investigated in 0.1 M PBS solution containing 2 mM ATCl. As could be seen from Fig. 8, the peak current of oxidation increased gradually with the increase of scanning rate. When the scanning rate increased, the relationship between the oxidation peak current and the square root of the scanning rate was linear (The inset image in Fig. 8). The oxidation peak current (Ia) versus the scan rate (ν) showed a linear relationship of I (μA) $= 0.07606\nu + 10.5075$ ($R^2 = 0.99576$). The anodic and cathodic peak currents were linearly proportional to the scan rates, which indicates that the electrocatalytic

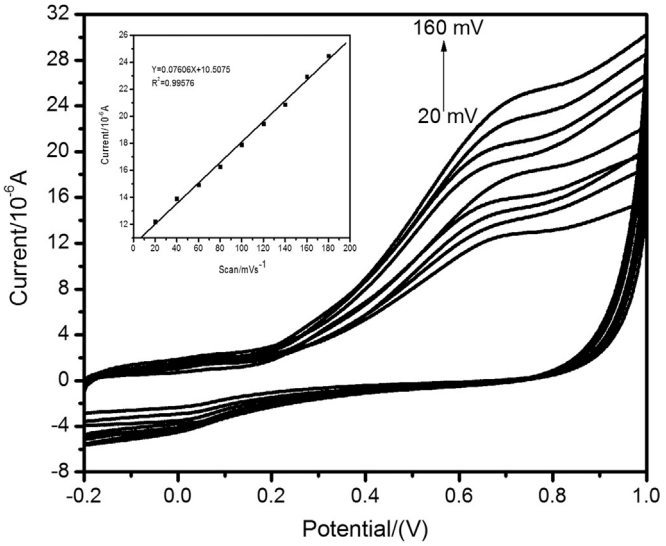

Fig. 8. CVs of GCE/P-ABSA/DAR/AuNPs/DAR/AChE electrode in 0.1 M PBS (pH 6.0) containing 2 mM ATCl at various scan rates (20–160 mV). Inset: the plot of the peak current versus scan rate.

behaviours of OPs are surface electron transfer processes.

3.7. Detection of pesticides

The GCE modified by P-ABSA/DAR/AuNPs/DAR/AChE was dipped sequentially in PBS solutions with different concentration of pesticide obtaining homologous cyclic voltammetry curves. As shown in Fig. 9(a and b), the oxidation peak currents of ATCl on GCE/P-ABSA/DAR/AuNPs/DAR/AChE were decreased with the concentration of malathion and methyl parathion increasing. The observed trend in the peak current could be assigned to the binding interaction of malathion and methyl parathion with the active target groups in enzyme, thus reducing the enzymatic activity to its substrate. The inset images in Fig. 9(a–b) show that both the attenuation of current and the concentration of pesticides follow a linear relationship of $Y = 3.24575X - 16.98509$ ($R^2 = 0.9894$) $X = -\log(\text{malathion})$ and $Y = 1.9123X - 8.25933$ ($R^2 = 0.992$) $X = -\log(\text{methyl parathion})$. A correlation between the current and inhibition rate (s) from this variation was determined in Fig. 10(a–b). A formula for the calculation of inhibition rate of AChE is obtained as follows:

$$\%Inhibition = (I_0 - I_1)/I_0 * 100\%$$

Where I_0 and I_1 denote the current in the absence and presence of OP_S respectively. %Inhibition versus $-\log$[malathion] and $-\log$[methyl parathion] followed a linear relationship of %Inhibition $= -13.05767X + 176.57778$ ($R^2 = 0.98626$) and %Inhibition $= -13.8X + 167.667$ ($R^2 = 0.992$). The detection limit (LD) of malathion and methyl parathion were calculated by using the equation given below:

$$LD = 3SB/b$$

SB is the standard deviation of the blank solution and b is the slope of the analytical curve. Figs. 9 and 10 showed a good inhibition rate of malathion and methyl parathion with a detection limit of 5.12×10^{-13} g L^{-1} for malathion and 5.85×10^{-13} g L^{-1} for methyl parathion. The analytical performance of malathion in the case of the resulting biosensor was compared with other reported AChE biosensors, and these results were summarised in Table 1. This shows that this biosensor had a wide detection range and a low detection limit.

3.8. Repeatability

The same enzyme electrode was detected once a day within a week in the presence of 10^{-10} g L^{-1} malathion in PBS solution containing 2 mM ATCl. The results were compared to reveal the repeatability of the OPs biosensor. The relative standard deviation (RSD) of OPs biosensor was found to be 4.37%, which proved a good repeatability. Additionally, the storage stability of the prepared biosensor was evaluated in 0.1M PBS at 4 °C. After the first 14-day storage, the biosensor in the presence of ATCl did not decrease obviously. Furthermore, after a 35-day storage period, the biosensor still retained 82% of its initial current response, thus demonstrating a desirable storage stability.

3.9. Real sample analysis with the proposed biosensor

To further investigate the potential practical application of the proposed biosensor to the analysis of real samples, the GCE/P-ABSA/DAR/AuNPs/DAR/AChE biosensor was used to monitor methyl parathion in tap water, well water and Chinese cabbage by the recovery test. The average recovery test was conducted by using the standard addition

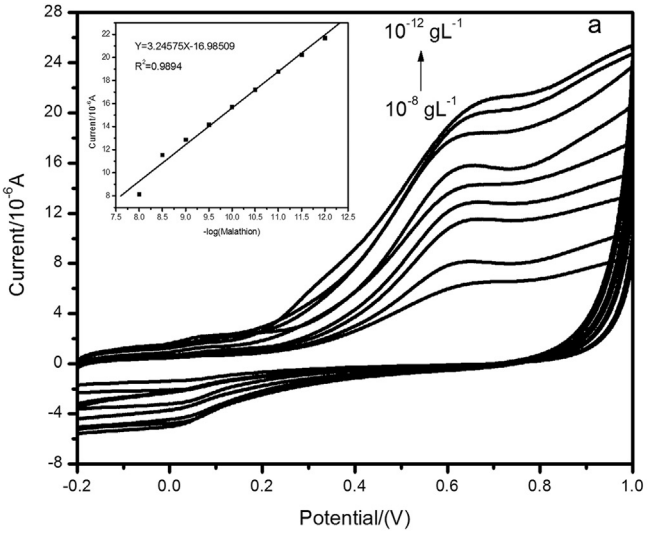

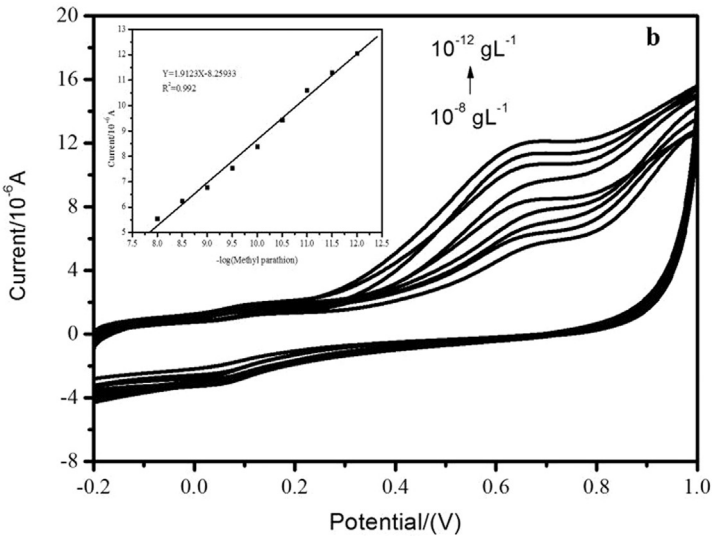

Fig. 9. a: CVs of GCE/P-ABSA/DAR/AuNPs/DAR/AChE in 0.1 M PBS (pH 6.0) containing 2 mM ATCl in malathion concentration range of 10^{-8}–10^{-12} g L^{-1}. Inset: the calibration curve between the attenuation of current and the concentration of malathion. **b:** CVs of GCE/P-ABSA/DAR/AuNPs/DAR/AChE in 0.1 M PBS (pH 6.0) containing 2 mM ATCl in methyl parathion concentration range of 10^{-8} –10^{-12} g L^{-1}. Inset: the calibration curve between the attenuation of current and the concentration of methyl parathion.

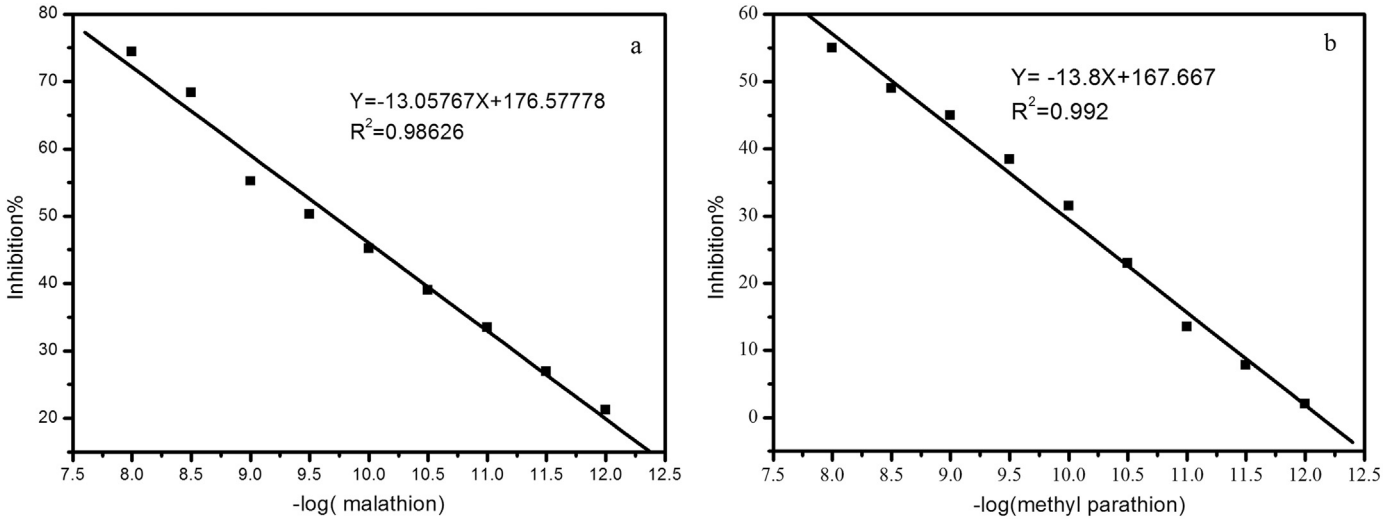

Fig. 10. a: The calibration curve between %Inhibition and the concentration of malathion. **b:** The calibration curve between %Inhibition and the concentration of methyl parathion.

Table 1
Comparison of the biosensor in this study with other reported AChE-based biosensors for OPs detection.

Sample	Electrode	Linear range	Detection Limit	Ref.
Malathion	AChE-Cs/Pd-Cu NWs/GCE	15–9,000,000 pM	4.5 pM	[38]
	AChE/PEDOT-MWCNTs/FTO	0.001–10,000,00 pM	0.001 pM	[39]
	AChE/CS-Ti_3C_2Tx/GCE	0.01–100,00 pM	0.003 pM	[40]
	GCE/P-ABSA/DAR/AuNPs/DAR/AChE	0.003–30 pM	0.0016 pM	This work
Methyl parathion	NF/AChE-CS/SnO_2NPs-CGR/GCE	0.1–10,000 pM	0.05 pM	[41]
	NF/AChE–CS/Pt NPs–CGR–NF/GCE	0.1–10,000 pM	0.05 pM	[42]
	NF/AChE/GNPs/CS/nano-PPCPE	0.038–38,000 pM	0.019 pM	[43]
	GCE/P-ABSA/DAR/AuNPs/DAR/AChE	0.0038–38 pM	0.0022 pM	This work

Table 2
Recovery tests of methyl parathion in tap water, well water and Chinese cabbage.

Sample	Added amount (g/L)	Measured amount (g/L)	Recovery (%)
Tap water	10^{-10} g/L	1.04×10^{-10} g/L	104%
	10^{-9} g/L	1.05×10^{-9} g/L	95%
Well water	10^{-10} g/L	0.96×10^{-10} g/L	96%
	10^{-9} g/L	0.95×10^{-9} g/L	95%
Chinese cabbage	10^{-10} g/L	0.97×10^{-10} g/L	106%
	10^{-9} g/L	0.96×10^{-9} g/L	97%

method, and these results are summarised in Table 2. This shows that the values of the recovery for the determination were in the range of 95–106%. Therefore, these further tests demonstrated that the biosensor exhibits excellent accuracy for the detection of OPs in real samples and consequently have significant potential for practical application.

4. Conclusion

In this paper, a novel stable covalently attached multilayer films was successfully constructed by using layer-by-layer self-assembly technique. Experimental results showed that the P-ABSA/DAR/AuNPs/DAR/AChE film exhibited excellent electron transfer mediation and electrical conductivity towards the pesticides in water. The biosensor possessed a low detection limit for both malathion and methyl parathion over a wide linear range with fine precision and reproducibility. The biosensor also showed good recovery in the analysis of real samples and thus has significant potential for practical application. Moreover, the storage stability testing of the biosensor revealed a high level of stability, indicating that the strong covalent bond used to modify the electrode also improved the stability of the biosensor compared with weak electrostatic force adsorption. It is anticipated that covalently attached multilayer assemblies could be used to fabricate stable enzyme biosensors in future research. The film simplified the electrode pretreatment and preparation processes compared with other preparation methods. Therefore, the film is suitable for the quantitative detection of trace OPs. This preparation method can also be extended to other proteins, enzymes and biomolecules fixed by functional AuNP/DAR films, which will greatly expand the use of biomolecules and nanomaterials in biosensor applications.

Acknowledgments

This paper was carried out at the ‘Northwest university research fund (Grant No. 338020015)’ under Northwest university, and was financially supported by scientific research plan projects of Education Department of Shaanxi Province (Grant No.203010019).

References

[1] P. Fantke, R. Charles, L. Felippe de Alencastro, R. Friedrich, O. Jollietd, Chemosphere 85 (2011) 1639–1647.
[2] D. Hamilton, S. Crossley, Wiley & Sons, 2004, pp. 1–25.
[3] A.R. Mulchandani, Rajesh, Biochem. Biotechnol. 165 (2011) 687–699.
[4] S. Chapalamadugu, G.S. Chaudhry, Crit. Rev. Biotechnol. 12 (1992) 357–389.
[5] D. Du, J. Wang, J.N. Smith, C. Timchalk, Y. Lin, Anal. Chem. 81 (2009) 9314–9320.
[6] G.L. Ellman, K.D. Courtney, V. Andres, Biochem. Pharmacol. 7 (1961) 88–95.
[7] A. Fidder, A.G. Hulst, D. Noort, R. de Ruiter, M.J. van der Schans, H.P. Benschop, J.P. Langenberg, Chem. Res. Toxicol. 15 (2002) 582–590.
[8] S. Walorczyk, J. Chromatogr. A 1165 (2007) 200–212.
[9] M.S. Kim, G.W. Kim, T.J. Park, Biosens. Bioelectron. 67 (2015) 408–412.
[10] S. Anandhakumar, K. Dhanalakshmi, J. Mathiyarasu, Electrochem. Commun. 38 (2014) 15–18.
[11] B. Hauser, M. Schellin, P. Popp, Anal. Chem. 76 (2004) 6029–6038.
[12] G. Jeanty, J.L. Marty, Biosens. Bioelectron. 13 (1998) 213–218.

[13] H. Chen, R. Chen, R. Feng, S. Li, Chromatographia 70 (2009) 165–172.
[14] Y. Li, Y. Bai, G. Han, M. Li, Sens. Actuators B 185 (2013) 706–712.
[15] Q. Zhou, L. Yang, G. Wang, Y. Yang, Biosens. Bioelectron. 49 (2013) 25–31.
[16] G. Liu, Y. Lin, Anal. Chem. 78 (2006) 835–843.
[17] A. Ivanov, G. Evtugyn, H. Budnikov, F. Ricci, D. Moscone, G. Palleschi, Anal. Bioanal. Chem. 377 (2003) 624–631.
[18] H.Y. Zhao, X.P. Jin, B.B. Wang, N. Wang, X.R. Li, R.X. Ni, J.J. Ren, Biosens. Bioelectron. 65 (2015) 23–30.
[19] J. Wang, Microchim. Acta 177 (2012) 245–270.
[20] E. Sapountzi, M. Braiek, F. Vocanson, J.F. Chateaux, N. Jaffrezic-Renault, F. Lagarde, Sens. Actuators B 238 (2017) 392–401.
[21] E. Lorencon, D.C. Ferreira, R.R. Resende, K. Krambrock, , Catal. A Gen. 505 (2015) 566–574.
[22] D.V. Jawale, E. Gravel, V. Geertsen, H. Li, N. Shah, R. Kumar, et al., Tetrahedron 70 (2014) 6140–6145.
[23] K. Saha, S.S. Agasti, C. Kim, X. Li, V.M. Rotello, Chem. Rev. 112 (2012) 2739–2779.
[24] S. Kumar, W. Ahlawat, R. Kumar, N. Dilbaghi, Biosens. Bioelectron. 70 (2015) 498–503.
[25] N. Dimcheva, E. Horozova, Y. Ivanov, T. Godjevargova, Cent. Eur. J. Chem. 11 (2013) 1740–1748.
[26] M. Wei, G.Y. Zeng, Q.Y. Lu, Microchim Acta 181 (2014) 121–127.
[27] W. Zhao, P.Y. Ge, J.J. XU, H.Y. Chen, Environ. Sci. Technol. 43 (2009) 6724–6729.
[28] D. Du, S.Z. Chen, J. Cai, A.D. Zhang, Talanta 74 (2008) 766–772.
[29] Y.R. Li, Z.Y. Gan, Y.F. Li, Q. Liu, J.C. Bao, Z.H. Dai, M. Han, Chem. Sci.Chin. 53 (2010) 820–825.
[30] Y.Y. Zhang, M.A. Arugula, J.S. Kirsch, X.Y. Yang, E. Olsen, A.L. Simonian, Langmuir 31 (2015) 1462–1468.
[31] Y. Lin, F. Lu, J. Wang, Electroanalysis 16 (2004) 145–149.
[32] J. Sun, T. Wu, F. Liu, Z. Wang, X. Zhang, J. Shen, Langmuir 16 (2000) 4620–4624.
[33] J. Sun, T. Wu, B. Zou, X. Zhang, J. Shen, Langmuir 17 (2001) 4035–4041.
[34] Y. Bai, S. Zhao, K. Zhang, C.Q. Sun, Colloids Surf. A Physicochem. Eng. Asp. 281 (2006) 105–112.
[35] X. Li, Y. Wan, C. Sun, Electroanal. Chem. 56 (2004) 79–87.
[36] K.C. Grabar, R.G. Freeman, M.B. Hommer, M.J. Natan, Anal. Chem. 67 (1995) 735–743.
[37] J.W. Cao, W.X. Cao, X.D. Feng, Chin. Sci. Bull. 20 (1989) 1709–1712.
[38] D.D. Song, Y. Li, X. Lu, M.X. Sun, H. Liu, G.M. Yu, F.M. Gao, Anal. Chim. Acta 982 (2017) 168–175.
[39] N. Kaur, H. Thakur, N. Prabhakar, J. Electroanal. Chem. 775 (2016) 121–128.
[40] L.Y. Zhou, X.N. Zhang, L. Ma, J. Gao, Y.N. Jiang, Biochem. Eng. J. 128 (2017) 243–249.
[41] Q. Zhou, L. Yang, G.C. Wang, Y. Yang, Biosens. Bioelectron. 49 (2013) 25–31.
[42] L. Yang, G.C. Wang, Y.J. Liu, Anal. Chem. 437 (2013) 144–149.
[43] Y. Deng, K.K. Liu, Y. Liu, H.M. Dong, S. Li, J. Nanosci. Nanotechnol. 16 (2016) 9460–9467.